



Article

All-Optical XOR, AND, OR, NOT, NOR, NAND, and XNOR Logic Operations Based on M-Shaped Silicon Waveguides at 1.55 μm

Amer Kotb^{1,2,*} , Kyriakos E. Zoiros³ and Wei Chen^{1,*}

¹ School of Chips, XJTLU Entrepreneur College (Taicang), Xi'an Jiaotong-Liverpool University, Taicang, Suzhou 215400, China

² Department of Physics, Faculty of Science, University of Fayoum, Fayoum 63514, Egypt

³ Lightwave Communications Research Group, Department of Electrical and Computer Engineering, School of Engineering, Democritus University of Thrace, 67100 Xanthi, Greece; kzoiros@ee.duth.gr

* Correspondence: amer.kotb@xjtlu.edu.cn (A.K.); wei.chen03@xjtlu.edu.cn (W.C.)

Abstract: Silicon waveguides are essential to integrated photonics, which is where optical and electronic components are coupled together on a single silicon chip. These waveguides allow for the integration of signal processing and optical transmission, which advances data centers, telecommunications, and other optical applications. Thus, our study involves the simulation of essential all-optical logic operations, namely XOR, AND, OR, NOT, NOR, NAND, and XNOR, and utilizes M-shaped silicon optical waveguides at a wavelength of 1.55 μm . This simulation is conducted through Lumerical FDTD solutions. The suggested waveguide comprises four identical slots, configured in the shape of the letter 'M', and all of which are formed of core silicon and silica cladding. These logic operations work based on constructive and destructive interferences that are caused by phase changes in the input optical beams. The contrast ratio (CR) is employed to quantitatively and comparatively assess the degree to which the target logic operations are efficiently executed. The simulation results indicate that, compared to other reported designs, the considered logic functions constructed using the proposed waveguide can be implemented with higher CRs. The outcomes of this paper can be utilized regarding the implementation of optoelectronic combinational logic circuits of enhanced functionality.

Keywords: optical logic operations; silicon-on-silica waveguide; contrast ratio



Citation: Kotb, A.; Zoiros, K.E.; Chen, W. All-Optical XOR, AND, OR, NOT, NOR, NAND, and XNOR Logic Operations Based on M-Shaped Silicon Waveguides at 1.55 μm .

Micromachines **2024**, *15*, 392.

<https://doi.org/10.3390/mi15030392>

Academic Editor: Maurizio Casalino

Received: 18 January 2024

Revised: 12 February 2024

Accepted: 12 March 2024

Published: 13 March 2024



Copyright: © 2024 by the authors. Licensee MDPI, Basel, Switzerland. This article is an open access article distributed under the terms and conditions of the Creative Commons Attribution (CC BY) license (<https://creativecommons.org/licenses/by/4.0/>).

1. Introduction

Silicon (Si) is widely utilized in the electronics industry as a semiconductor, making it a crucial material in the production of computer chips, solar cells, waveguides, etc. Silica refers to silicon dioxide (SiO_2), a compound made up of silicon and oxygen atoms. It is one of the most abundant compounds on Earth and is found in various forms, such as quartz, sand, and agate. Si waveguides, on the other hand, are typically made of silicon-on-insulator (SOI) substrates, where a thin layer of silicon is sandwiched between layers of SiO_2 . These waveguides guide light through the Si core by exploiting the refractive index contrast between Si and the surrounding SiO_2 . The high refractive index of Si ensures that the light is confined within the Si core, preventing it from spreading into the cladding. Si waveguides are applied in various fields, including telecommunications, data communications, optical interconnects, and sensors. They play a crucial role in connecting different components on a photonic integrated circuit, such as lasers, modulators, detectors, and other passive elements. Additionally, Si waveguides offer several advantages, including compatibility with existing CMOS technology, which enables cost-effective manufacturing. They also allow for the integration of photonics with existing electronic integrated circuits on a single chip, creating opportunities for more efficient and compact devices [1–8]. On the other hand, optical logic operations can have potential advantages in terms of speed and energy efficiency as compared to traditional electronic circuits [9,10]. Indeed, optical logic

gates have recently been designed and/or constructed utilizing a variety of waveguide designs [11–41]. Implementing complete optical computing systems based on optical logic functions is a challenging task because it involves maintaining signal integrity over long distances, dealing with issues such as signal loss and dispersion, and developing practical devices that can be integrated into larger systems. The compact Si waveguide that we propose in this work is capable of executing seven optical logic operations (XOR, AND, OR, NOT, NOR, NAND, and XNOR) at $1.55\ \mu\text{m}$ simultaneously, while the majority of the other reported designs have used photonic crystals (PhCs) [11–22] or noble metals [32–37] to implement only one or, at most, two logic operations. Four identical slots, configured in the shape of the letter ‘M’, comprise the suggested waveguide; these slots are all composed of Si on top of SiO_2 . Compared to our previous Si designs [26–31], this proposed waveguide is easier to use in the communications network, as well as in the design of many computational logic circuits. The variety of waveguide designs allows engineers and designers to choose the most appropriate structure for a given application, taking into account factors like frequency range, mode handling, size, polarization, materials, manufacturing constraints, and specialized requirements. This versatility enables the optimization of performance and efficiency in a wide range of electromagnetic wave-based systems. In this paper, the logic operations work is based on constructive interference (CI) and destructive interference (DI) that results from the input optical beams’ phase variations. The performance of the logic operations is evaluated utilizing the contrast ratio (CR) metric [26–31] through Lumerical finite-difference-time-domain (FDTD) solutions [42], with the convolutional perfectly matched layer (PML) as an absorbing boundary condition [43]. The incident light will be absorbed with a minimal number of reflections under the PML absorbing boundary conditions. However, spurious numerical reflections occur in a discretized FDTD space even when the PML is perfectly capable of absorbing incident beams. The coordinate stretching variables inside the PML might be graded to lessen these reflections [43]. In this case, the XYZ axis mesh accuracy is set to $0.05\ \mu\text{m}$, $0.05\ \mu\text{m}$, and $0.01\ \mu\text{m}$, respectively. The simulation findings show that the examined logic functions generated when using the suggested waveguide can be achieved with higher CRs when compared to other reported designs [11,16–18,22,23,34,35,40,41] (see Table 8). These findings complement and generalize our relevant research that has been conducted so far [26–31], and essentially extends the technological suite in the quest for providing different design and building options for Si waveguide-based core logic modules.

2. Waveguide Principle

Figure 1 depicts the schematic illustration and electric field intensity distributions of the proposed waveguide, which is made up of four identical slots configured in the shape of the letter ‘M’, all of which are implemented on an SOI platform of a core Si layer and SiO_2 cladding. All slots have a fixed length (L) of $1.0\ \mu\text{m}$, width (w) of $0.22\ \mu\text{m}$, thickness (d) of $0.3\ \mu\text{m}$, and angle (θ) of 60° . The FDTD simulations have been run iteratively until we were strongly confident about their applicability and validity.

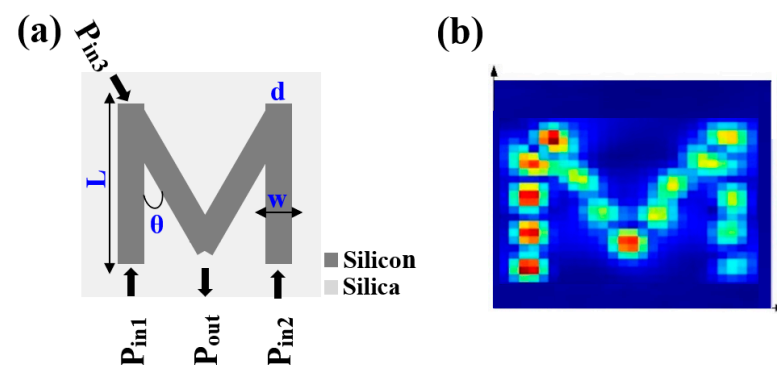


Figure 1. (a) Schematic illustration and (b) electric field intensity distributions of M-shaped Si waveguide.

The spectral transmission (T) of Si depends on the thickness of the Si wafer and the specific type of Si (e.g., crystalline or amorphous). Crystalline Si has good transmission in the infrared region, but it starts to absorb light in the visible and ultraviolet regions. A transverse magnetic (TM) mode polarized pulse at $1.55\ \mu\text{m}$ excites the input ports. The outcomes of the simulations are captured by setting FDTD monitors, i.e., $T = I_{\text{out}}/I_{\text{in}} = |E_{\text{out}}|^2/|E_{\text{in}}|^2$, where I_{out} is the intensity at the output port (i.e., port 4), and $I_{\text{in}} = I_1 + I_2 + I_3$, which is the sum of the intensities at three input ports [26–31]. The value of 0.2 is assigned to the normalized threshold transmission (T_{th}), which is the minimum normalized power required to generate T . To optimize T , the incident beams have to meet suitable phase-matching conditions [44,45]. From a logical perspective, port 4 produces an output of ‘1’ only if $T > T_{\text{th}}$ and ‘0’ if $T \leq T_{\text{th}}$.

The interaction between silicon waveguides and an incident optical signal is typically described by the phenomenon of mode coupling [46–48]. Mode coupling refers to the interaction between different guided modes within the waveguide structure. When an incident signal encounters a waveguide, it can excite various guided modes depending on factors such as wavelength, polarization, and the waveguide’s geometric and refractive index properties. In the context of silicon waveguides, the interaction involves the coupling of the incident signal to specific guided modes supported by the waveguide. These guided modes can include fundamental modes (e.g., TE or TM modes) and higher-order modes, each with its unique spatial distribution of the electric field within the waveguide. Understanding and controlling mode coupling is crucial for designing efficient photonic devices and circuits. Engineers and researchers use numerical simulations, as well as experimental techniques, to analyze and optimize mode coupling in silicon waveguides for specific applications, such as signal routing, modulation, waveguides, and detection in integrated optical systems.

In Figure 2, the illustration specifically showcases how the normalized spectral transmission (T) of the M-shaped silicon waveguide varies with the operating wavelength (λ), assuming that all incident beams are uniformly launched at the three input ports with the same phase of 180° . At the wavelength of $1.55\ \mu\text{m}$, the proposed waveguide demonstrates an impressive high T of 0.894. A more detailed examination of the figure emphasizes that this waveguide consistently operates with high T over a broader wavelength spectrum, spanning from $1.2\ \mu\text{m}$ to $1.6\ \mu\text{m}$. This extended range underscores the versatility and reliability of the waveguide’s performance across different wavelengths, making it a promising candidate for various optical applications.

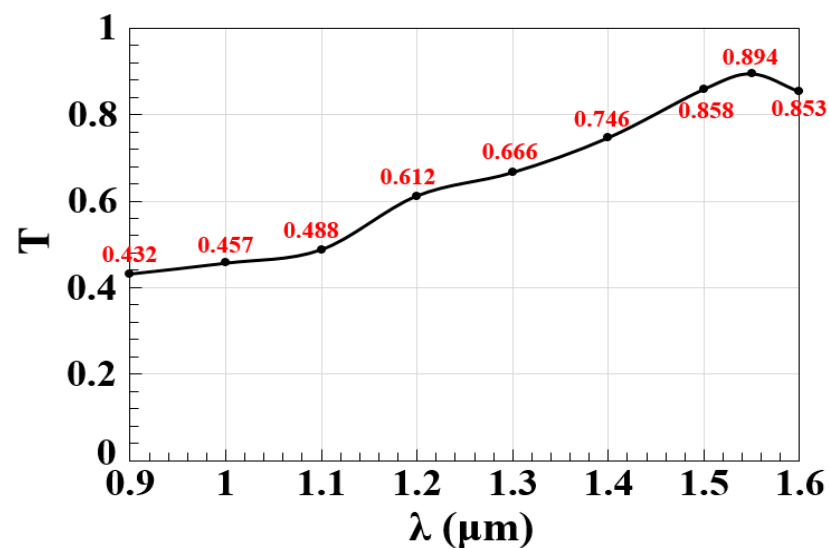


Figure 2. T versus λ using the M-shaped Si waveguide at $1.55\ \mu\text{m}$.

The angle between slots (i.e., θ) may affect how light or signals are manipulated within the waveguide. The effect of θ on T at $1.55 \mu\text{m}$ is thus simulated in Figure 3. Upon the examination of this figure, it is evident that the maximum $T = 0.894$ is achieved at $\theta = 60^\circ$. Consequently, this is the optimum value specified for θ , which is accordingly used as fixed throughout our simulations. Expanding on this figure, it is also evident that altering the value of θ results in an increase in the light scattering and absorption within the materials, thereby reducing T .

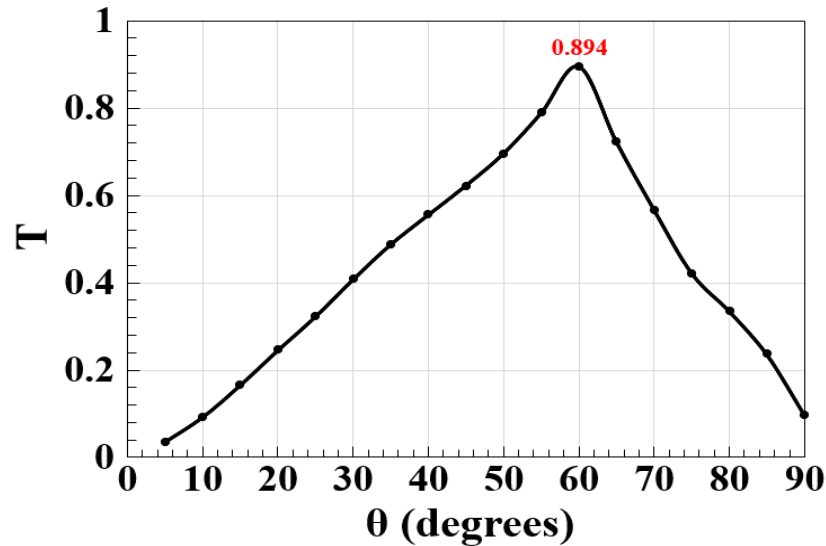


Figure 3. T versus θ using the M-shaped Si waveguide at $1.55 \mu\text{m}$.

The dimensions of a Si waveguide can significantly impact its performance, especially in the context of integrated photonics. For example, the length of the waveguide influences the overall propagation losses. Longer waveguides tend to have higher losses, and minimizing the length is often crucial for device efficiency. A more narrow waveguide tends to have lower losses [49]. Therefore, Figure 4 illustrates how the slot length (L) and width (w) affect T . As seen in this figure, high T is produced by the suggested Si waveguide across a broad range of L and w , or $L = 0.5\text{--}2.5 \mu\text{m}$ and $w = 0.1\text{--}0.5 \mu\text{m}$.

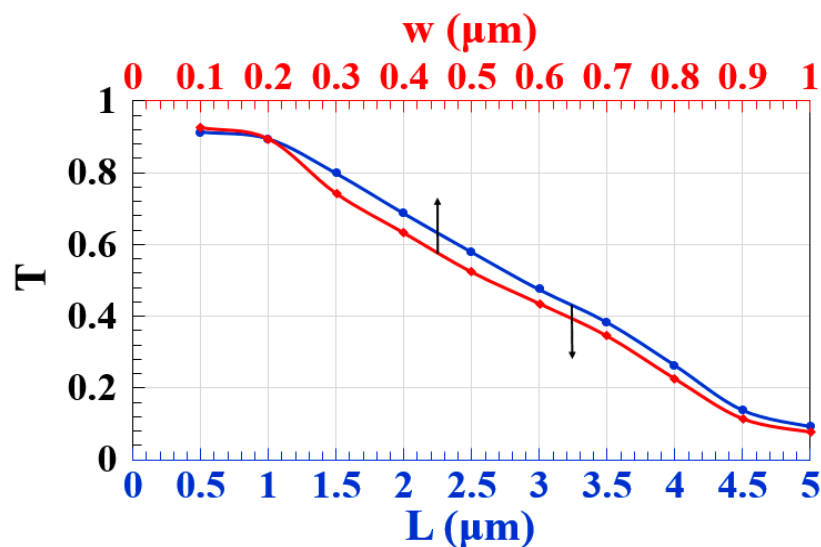


Figure 4. T versus L and w using the M-shaped Si waveguide at $1.55 \mu\text{m}$.

3. Logic Operations

3.1. XOR, AND, OR

Two input beams are injected into P_{in2} and P_{in3} , and P_{in1} must supply a clock beam (CLK) with an angle of 180° to execute the XOR, AND, and OR logic operations. Establishing a reference phase difference between input beams that results in either CI or DI can be done using the CLK (all '1's). A '1' output is produced by CI when all input beams are launched with the same phase, but a '0' output is produced by DI when these beams exhibit different phases. It is noteworthy to observe that the output logic operation occurs in between the two signals launched into the proposed waveguide from P_{in2} and P_{in3} . Using the M-shaped Si waveguide at $1.55 \mu\text{m}$, the field intensity distributions of the XOR, AND, and OR operations are shown in Figures 5–7, respectively.

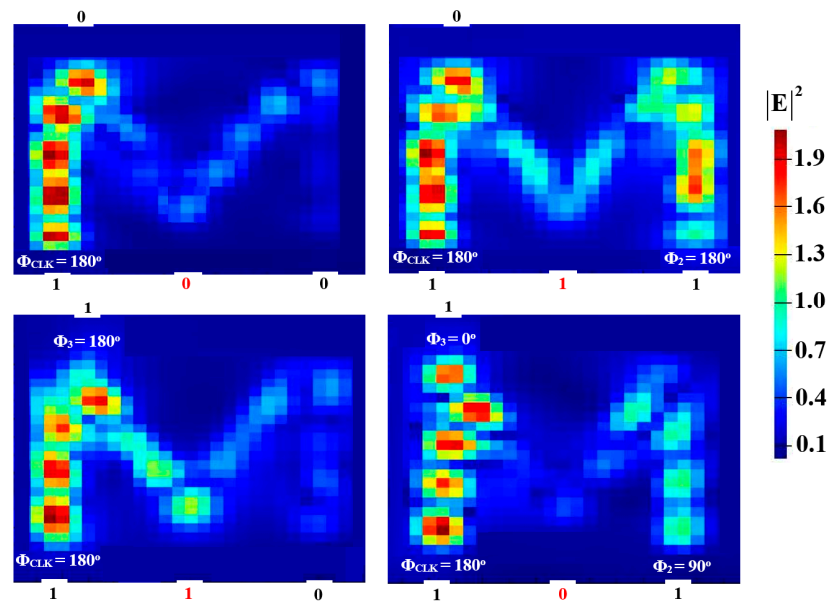


Figure 5. XOR field intensity distributions using the M-shaped Si waveguide at $1.55 \mu\text{m}$.

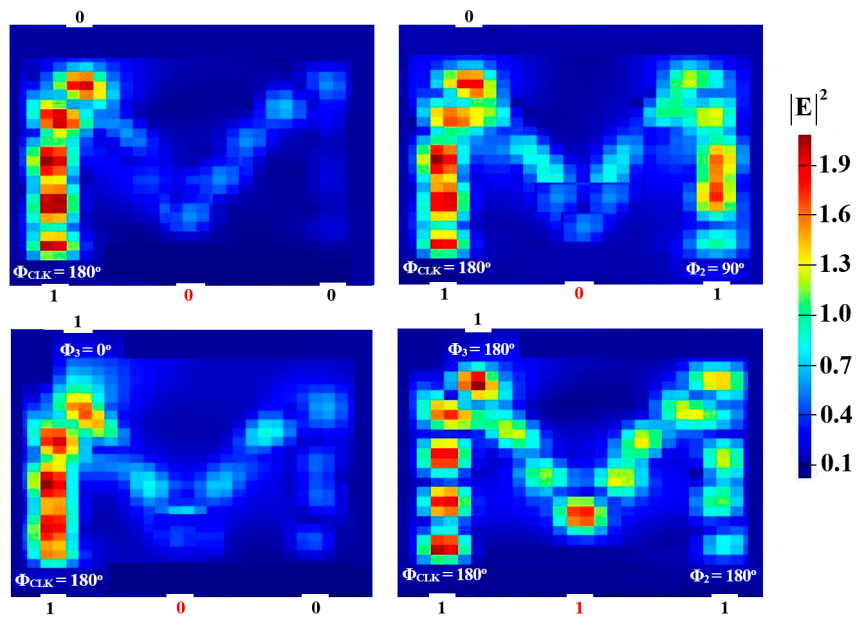


Figure 6. AND field intensity distributions using the M-shaped Si waveguide at $1.55 \mu\text{m}$.

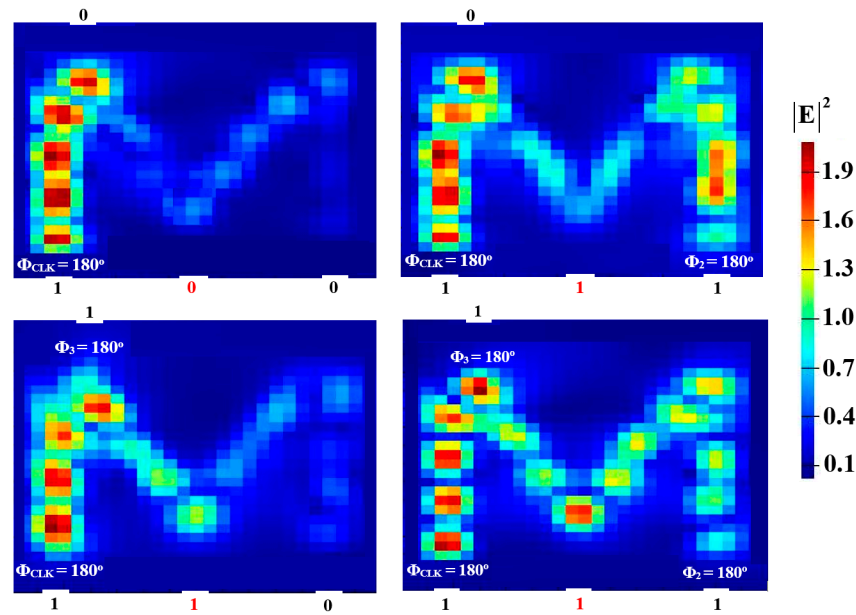


Figure 7. OR field intensity distributions using the M-shaped Si waveguide at 1.55 μm .

The suggested waveguide proved successful in achieving a high CR. The simulation results for the AND, OR, and XOR logic operations at 1.55 μm in terms of T and CR are summarized in Tables 1–3, respectively.

Table 1. XOR simulation results ($T_{\text{th}} = 0.20$).

Φ_{CLK}	Φ_2	Φ_3	P_{out}	T	CR (dB)
180°	-	-	0	0.024	
180°	180°	-	1	0.586	14.94
180°	-	180°	1	0.786	
180°	90°	0°	0	0.021	

Table 2. AND simulation results ($T_{\text{th}} = 0.20$).

Φ_{CLK}	Φ_2	Φ_3	P_{out}	T	CR (dB)
180°	-	-	0	0.024	
180°	90°	-	0	0.028	15.36
180°	-	0°	0	0.026	
180°	180°	180°	1	0.894	

Table 3. OR simulation results ($T_{\text{th}} = 0.20$).

Φ_{CLK}	Φ_2	Φ_3	P_{out}	T	CR (dB)
180°	-	-	0	0.024	
180°	180°	-	1	0.586	15.20
180°	-	180°	1	0.786	
180°	180°	180°	1	0.894	

3.2. NOT, NOR, NAND, XNOR

In order to perform NOT, NOR, NAND, and XNOR logic operations, a Clk with $\Phi_{\text{CLK}} = 0^\circ$ is injected into $P_{\text{in}3}$, while two beams are injected into $P_{\text{in}1}$ and $P_{\text{in}2}$ (see Figure 1). When the input beams are launched at different angles, they interact destructively and incur a logical ‘0’ at $P_{\text{in}4}$. However, when launched at identical angles, they interfere constructively and make a logical ‘1’ appear at $P_{\text{in}4}$. Figures 8–11 display the field intensity distribu-

tions of the NOT, NOR, NAND, and XNOR operations, respectively, using the suggested Si waveguide at 1.55 μm .

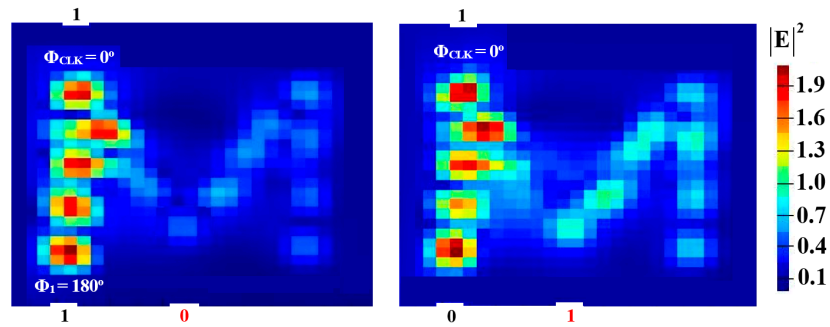


Figure 8. NOT field intensity distributions using the M-shaped Si waveguide at 1.55 μm .

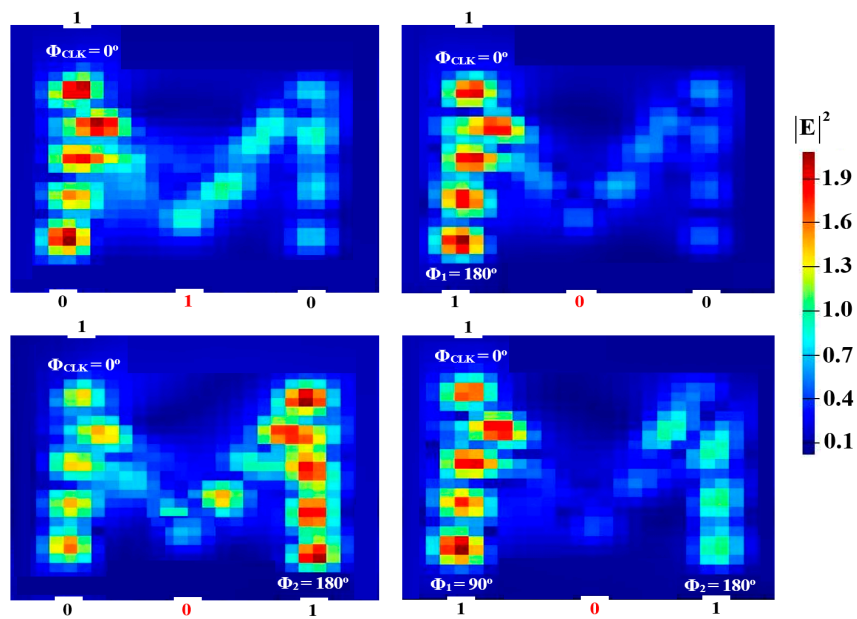


Figure 9. NOR field intensity distributions using the M-shaped Si waveguide at 1.55 μm .

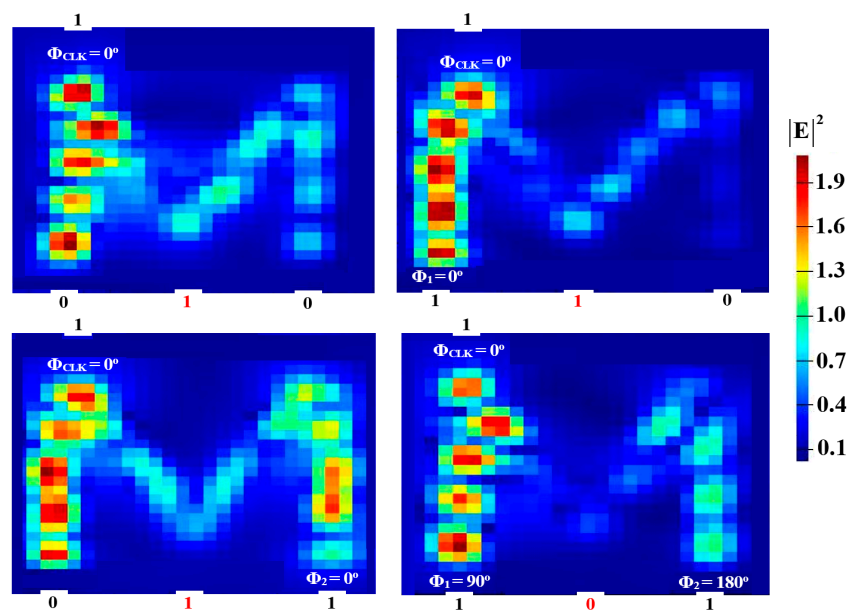


Figure 10. NAND field intensity distributions using the M-shaped Si waveguide at 1.55 μm .

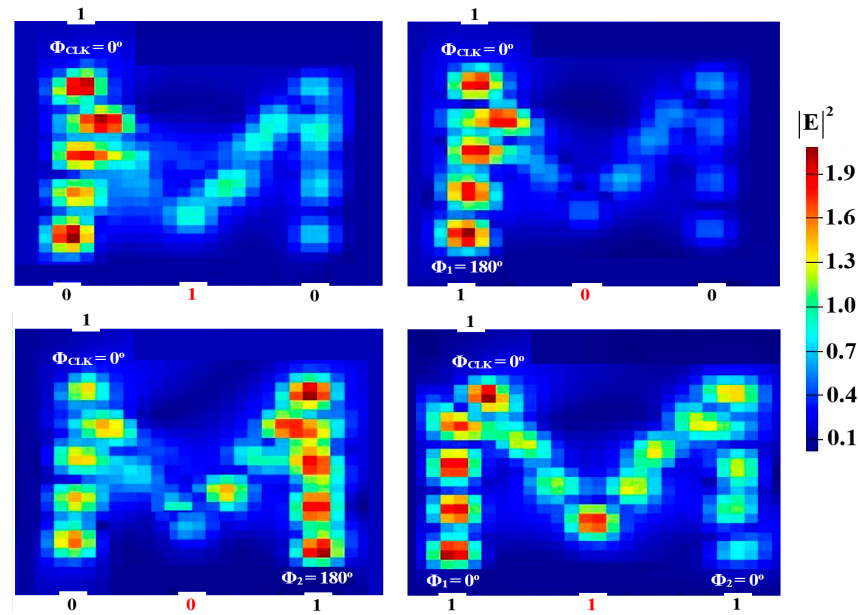


Figure 11. XNOR field intensity distributions using the M-shaped Si waveguide at 1.55 μm .

Tables 4–7 provide a summary of the simulation findings for the NOT, NOR, NAND, and XNOR operations at 1.55 μm , respectively. These tables indicate that our design achieves acceptable performance.

Table 4. NOT simulation results ($T_{\text{th}} = 0.20$).

Φ_1	Φ_{CLK}	P_{out}	T	CR (dB)
180°	0°	0	0.024	15.10
-	0°	1	0.775	

Table 5. NOR simulation results ($T_{\text{th}} = 0.20$).

Φ_1	Φ_2	Φ_{CLK}	P_{out}	T	CR (dB)
-	-	0°	1	0.775	15.28
180°	-	0°	0	0.024	
-	180°	0°	0	0.026	
90°	180°	0°	0	0.021	

Table 6. NAND simulation results ($T_{\text{th}} = 0.20$).

Φ_1	Φ_2	Φ_{CLK}	P_{out}	T	CR (dB)
-	-	0°	1	0.775	14.65
0°	-	0°	1	0.575	
-	0°	0°	1	0.484	
90°	180°	0°	0	0.021	

Table 7. XNOR simulation results ($T_{\text{th}} = 0.20$).

Φ_1	Φ_2	Φ_{CLK}	P_{out}	T	CR (dB)
-	-	0°	1	0.775	15.24
180°	-	0°	0	0.024	
-	180°	0°	0	0.027	
0°	0°	0°	1	0.894	

A comparison of our waveguide with the other published designs-based optical logic operations [11,16–18,22,23,34,35,40,41] is given in Table 8. This comparison includes both

theoretical and practical results using various optical structures. This table proves that the suggested design has several advantages, such as being created with cost-effective materials like Si and SiO₂, as well as being more compact, and providing a better performance. Additionally, with the possibility of designing using electron beam lithography or laser techniques, the suggested design enables seamless integration with electronic components on a single chip. These advantages make our compact waveguides a popular choice in the development of integrated photonic circuits for other optical applications.

Table 8. Comparison of proposed and other waveguide-based waveguides of optical logic functions.

References	Functions	Design	Materials	Size (μm^2)	Wavelength (nm)	CR (dB)
[11]	AND, XOR, OR, NOT, NAND, NOR, XNOR	PhC waveguides	Si/air	9×5	1550	5.42–9.59
[16–18]	AND, XOR, XNOR	T-shaped PhC waveguides	Si/air	-	1550	8.29–33.05
[22]	AND, OR	2D PhC design	Si/air	19.8×12.6	1520	9.74 and 17.95
[23]	AND, NOR, XNOR	Si photonics platform			1550	>10 dB
[34]	NOT, XOR, AND, OR, NOR, NAND, XNOR	Metal slot waveguide	Silver/SiO ₂	1.5×2.36	632.8	6–16
[35]	NOT, XOR, AND, OR, NOR, NAND, XNOR	Metal-insulator-metal structures	Air/silver	5.33×0.42	632.8	15
[40]	AND, NAND, OR, XOR, NOR, XNOR, NOT	Plasmonic logic gates design	Silver/SiO ₂	0.25×0.25	850	4.14–14.46
[41]	AND, OR, NOT, NAND	Inverse design on Si platforms	Si/SiO ₂	1.0×1.5	1300	0.5–5.79
This work	XOR, AND, OR, NOT, NOR, XNOR, NAND	M-shaped Si waveguides	Si/SiO ₂	1.0×1.0	1550	14.65–15.36

Fabricating nanometer-scale waveguides demands sophisticated techniques in micro-fabrication and nanotechnology. Key methodologies, such as advanced photolithography (e.g., extreme ultraviolet lithography or electron beam lithography), are pivotal for crafting silicon-on-silica waveguides. Achieving high precision and control in optical structure creation is facilitated by femtosecond direct writing. Etching processes, like reactive ion etching or deep reactive ion etching, play a crucial role in precisely shaping silicon and forming the intricate waveguide structures. The deposition of thin silicon layers on silica substrates can be achieved through either chemical vapor deposition or physical vapor deposition. It's worth noting that the selection of specific techniques depends on the unique requirements of the waveguide design, as well as the available fabrication facilities. In this dynamic field, staying abreast of the latest research and developments in nanotechnology and microfabrication is imperative. It is noteworthy that ongoing advancements in these technologies continually unfold, emphasizing the importance of remaining current with emerging methodologies. Despite the intricacies involved, the experimental validation of the proposed waveguide is within reach due to the accessibility of an advanced manufacturing processes. Rather than presenting an insurmountable obstacle, the fabrication challenge becomes a practical matter with potential solutions. Furthermore, recent reports highlight successful experimental implementations of multiple optical logic gates based on various optical waveguides. These findings, documented in references [23,32,34,50–58], signify a significant stride forward and pave the way for analogous implementations in the future. The footprint of other waveguide-based implementations of optical logic gates is even smaller, as reported, for instance, in reference [40] and cited in the corresponding column of Table 8.

4. Conclusions

We have proposed and demonstrated, through Lumerical FDTD simulations, all-optical XOR, AND, OR, NOT, NOR, NAND, and XNOR logic operations at 1.55 μm using four identical slots configured in the shape of the letter 'M', all of which are formed of

core Si and SiO₂ cladding. The constructive and destructive interferences that result from the phase shifts, induced by the inserted input optical beams, constitute the fundamental principles for the physical realization of these logic operations. According to the theoretical findings, the suggested waveguide allows for the construction of the target logic operations while exhibiting higher CRs than other reported designs. The outcomes of this work can open new possibilities for the practical design and implementation of optoelectronic combinational logic circuits of advanced functionality.

Author Contributions: Conceptualization, A.K.; Data curation, A.K.; Formal analysis, A.K.; Funding acquisition, A.K.; Investigation, A.K. and K.E.Z.; Methodology, A.K.; Project administration, A.K.; Resources, A.K.; Lumerical FDTD Software, A.K.; Supervision, W.C.; Writing—original draft, A.K.; Writing—review & editing, A.K., K.E.Z. and W.C. All authors have read and agreed to the published version of the manuscript.

Funding: This research received no external funding.

Data Availability Statement: Data are contained within the article.

Conflicts of Interest: The authors declare no conflict of interest.

References

- Chen, L.R.; Wang, J.; Naghdi, B.; Glesk, I. Subwavelength grating waveguide devices for telecommunications applications. *IEEE J. Sel. Top. Quantum Electron.* **2019**, *25*, 8200111. [[CrossRef](#)]
- Lipson, M. Guiding, modulating, and emitting light on silicon—challenges and opportunities. *J. Light. Technol.* **2005**, *23*, 4222–4238. [[CrossRef](#)]
- Vlasov, Y.A. Silicon photonics for next-generation computing systems. In Proceedings of the 34th European Conference on Optical Communication (ECOC 2008), Brussels, Belgium, 21–25 September 2008; paper Tu.1.A.1.
- Lee, B.G.; Bergmann, K. Silicon nano-photonic interconnection networks in multicore processor systems. In Proceedings of the Optical Society of America (OSA) Annual Meeting, Toronto, ON, Canada, 3–8 October 2008; paper FTth S1.
- Thourhout, D.V.; Campenhout, J.V.; Baets, R.; Rojo-Romeo, P.; Regreny, P.; Seassal, C.; Binetti, P.; Leijtens, X.J.M.; Ntzel, R.; Smit, M.K.; et al. Photonic interconnect layer on CMOS. In Proceedings of the 33rd European Conference and Exhibition on Optical Communication, Berlin, Germany, 16–20 September 2007; paper 6.3.1.
- Tsybeskov, L.; Lockwood, D.J.; Ichikawa, M. Silicon photonics: CMOS going optical. *Proc. IEEE* **2009**, *97*, 1161–1165. [[CrossRef](#)]
- Shi, Y.; Zhang, Y.; Wan, Y.; Yu, Y.; Zhang, Y.; Hu, X.; Xiao, X.; Xu, H.; Zhang, L.; Pan, B. Silicon photonics for high-capacity data communications. *Photon. Res.* **2022**, *10*, A106–A134. [[CrossRef](#)]
- Tsuchizawa, T.; Yamada, K.; Fukuda, H.; Watanabe, T.; Takahashi, J.; Takahashi, M.; Shoji, T.; Tamechika, E.; Itabashi, S.; Morita, H.; et al. Microphotonics devices based on silicon microfabrication technology. *IEEE J. Sel. Top. Quantum Electron.* **2005**, *11*, 232–240. [[CrossRef](#)]
- Saruwatari, A. All-optical signal processing for terabit/second optical transmission. *IEEE J. Sel. Top. Quantum Electron.* **2000**, *6*, 1363–1374. [[CrossRef](#)]
- Willner, A.E.; Khaleghi, S.; Chitgarha, M.R.; Yilmaz, O.F. All-optical signal processing. *J. Light. Technol.* **2014**, *32*, 660–680. [[CrossRef](#)]
- Rani, P.; Kalra, Y.; Sinha, R.K. Design of all optical logic gates in photonic crystal waveguides. *Optik* **2015**, *126*, 950–955. [[CrossRef](#)]
- Husko, C.; Vo, T.D.; Corcoran, B.; Li, J.; Krauss, T.; Eggleton, B. Ultracompact all-optical XOR logic gate in a slow-light silicon photonic crystal waveguide. *Opt. Express* **2011**, *19*, 20681–20690. [[CrossRef](#)]
- Andalib, P.; Granpayeh, N. All-optical ultracompact photonic crystal AND gate based on nonlinear ring resonators. *J. Opt. Soc. Am. B* **2009**, *26*, 10–16. [[CrossRef](#)]
- Jandieri, V.; Khomeriki, R.; Erni, D. Realization of true all-optical AND logic gate based on the nonlinear coupled air-hole type photonic crystal waveguide. *Opt. Express* **2018**, *26*, 19845–19853. [[CrossRef](#)]
- Ishizaka, Y.; Kawaguchi, Y.; Saitoh, K.; Koshihara, M. Design of ultracompact all-optical XOR and AND logic gates with low power consumption. *Opt. Commun.* **2011**, *284*, 3528–3533. [[CrossRef](#)]
- Priya, N.H.; Swarnakar, S.; Krishna, S.V.; Kumar, S. Design and analysis of an optical three-input AND gate using a photonic crystal fiber. *Appl. Opt.* **2022**, *61*, 77–83.
- Priya, N.H.; Swarnakar, S.; Krishna, S.V.; Kumar, S. Design and analysis of a photonic crystal-based all-optical 3-input OR gate for high-speed optical processing. *Opt. Quantum Electron.* **2021**, *53*, 720. [[CrossRef](#)]
- Rao, D.G.S.; Swarnakar, S.; Palacharla, V.; Raju, K.S.R.; Kumar, S. Design of all-optical AND, OR, and XOR logic gates using photonic crystals for switching applications. *Photon. Netw. Commun.* **2021**, *41*, 109–118. [[CrossRef](#)]
- Swarnakar, S.; Palacharla, V.; Muduli, A.; Kumar, S. Design and optimization of photonic crystal based all-optical logic gate with enhanced contrast ratio. *Opt. Quantum Electron.* **2023**, *55*, 623. [[CrossRef](#)]

20. Rachana, M.; Swarnakar, S.; Babu, M.R.; Swetha, P.M.; Rangaiah, Y.P.; Krishna, S.V.; Kumar, S. Optimization of an all-optical 3-input universal logic gate with an enhanced contrast ratio by exploiting T-shaped photonic crystal waveguide. *App. Opt.* **2022**, *61*, 8162–8171. [[CrossRef](#)] [[PubMed](#)]
21. Pavelyev, V.; Krivosheeva, Y.; Golovashkin, D. Genetic optimization of the Y-shaped photonic crystal NOT logic gate. *Photonics* **2023**, *10*, 1173. [[CrossRef](#)]
22. Mostafa, T.S.; Mohammed, N.A.; El-Rabaie, E.M. Ultra-high bit rate all-optical AND/OR logic gates based on photonic crystal with multi-wavelength simultaneous operation. *J. Mod. Opt.* **2019**, *66*, 1005–1016. [[CrossRef](#)]
23. Kita, S.; Nozaki, K.; Takata, K.; Shinya, A.; Notomi, M. Ultrashort low-loss Ψ gates for linear optical logic on Si photonics platform. *Commun. Phys.* **2020**, *3*, 33. [[CrossRef](#)]
24. Zeng, S.; Zhang, Y.; Pun, E. Ultrasmall optical logic gates based on silicon periodic dielectric waveguides. *Photon. Nanostr. Fundam. Appl.* **2010**, *8*, 32. [[CrossRef](#)]
25. Cui, L.; Yu, L. Multifunctional logic gates based on silicon hybrid plasmonic waveguides. *Mod. Phys. Lett. B* **2018**, *32*, 1850008. [[CrossRef](#)]
26. Kotb, A.; Zoiros, K.E.; Hatziefremidis, A.; Guo, C. Optical logic gates based on Z-shaped silicon waveguides at 1.55 μm . *Micromachines* **2023**, *14*, 1266. [[CrossRef](#)] [[PubMed](#)]
27. Kotb, A.; Zoiros, K.E.; Li, W. Silicon-on-silica waveguides-based all-optical logic gates at 1.55 μm . *Phys. Scr.* **2023**, *98*, 035517. [[CrossRef](#)]
28. Kotb, A.; Yao, C. All-optical logic operations based on silicon-on-insulator waveguides. *Opt. Eng.* **2023**, *62*, 048101. [[CrossRef](#)]
29. Kotb, A.; Zoiros, K.E. 2×2 compact silicon waveguide-based optical logic functions at 1.55 μm . *Photonics* **2023**, *10*, 403. [[CrossRef](#)]
30. Kotb, A.; Zoiros, K.E.; Guo, C. All-optical logic gates using E-shaped silicon waveguides at 1.55 μm . *J. App. Phys.* **2023**, *133*, 173101. [[CrossRef](#)]
31. Kotb, A.; Zoiros, K.E.; Guo, C. High-performance all-optical logic operations using ψ -shaped silicon waveguides at 1.55 μm . *Micromachines* **2023**, *14*, 1793. [[CrossRef](#)]
32. Gao, L.; Chen, L.; Wei, H.; Xu, H. Lithographically fabricated gold nanowire waveguides for plasmonic routers and logic gates. *Nanoscale* **2018**, *10*, 14771. [[CrossRef](#)]
33. Nozhat, N.; Alikomak, H.; Khodadadi, M. All-optical XOR and NAND logic gates based on plasmonic nanoparticles. *Opt. Commun.* **2017**, *392*, 208–213. [[CrossRef](#)]
34. Pan, D.; Wei, H.; Xu, H. Optical interferometric logic gates based on metal slot waveguide network realizing whole fundamental logic operations. *Opt. Express* **2013**, *21*, 9556. [[CrossRef](#)]
35. Bian, Y.; Gong, Q. Compact all-optical interferometric logic gates based on one-dimensional metal-insulator-metal structures. *Opt. Commun.* **2014**, *313*, 27–35. [[CrossRef](#)]
36. Al-Musawi, H.K.; Al-Janabi, A.K.; Al-Abassi, S.A.W.; Abusiba, N.A.A.; Al-Fatlawi, N.A.Q. Plasmonic logic gates based on dielectric-metal-dielectric design with two optical communication bands. *Optik* **2020**, *223*, 165416. [[CrossRef](#)]
37. Yao, C.; Kotb, A.; Wang, B.; Singh, S.; Guo, C. All-optical logic gates using dielectric-loaded waveguides with quasi-rhombus metasurfaces. *Opt. Lett.* **2020**, *45*, 3769–3772. [[CrossRef](#)]
38. Keshtkar, P.; Miri, M.; Yasrebi, N. Low power, high speed, all-optical logic gates based on optical bistability in graphene-containing compact microdisk resonators. *Appl. Opt.* **2021**, *60*, 7234–7242. [[CrossRef](#)]
39. Kotb, A.; Guo, C. 100 Gb/s all-optical multifunctional AND, XOR, NOR, OR, XNOR, and NAND logic gates in a single compact scheme based on semiconductor optical amplifiers. *Opt. Laser Technol.* **2021**, *137*, 106828. [[CrossRef](#)]
40. Alali, M.J.; Raheema, M.N.; Alwahib, A.A. Nanoscale plasmonic logic gates design by using an elliptical resonator. *App. Opt.* **2023**, *62*, 4080–4088. [[CrossRef](#)]
41. Neseli, B.; Yilmaz, Y.A.; Kurt, H.; Turdnev, M. Inverse design of ultra-compact photonic gates for all-optical logic operations. *J. Phys. D Appl. Phys.* **2022**, *55*, 215107. [[CrossRef](#)]
42. Available online: <https://www.ansys.com/products/optics/fdtd> (accessed on 31 December 2018).
43. Laakso, I.S.; Ilvonen, S.T.; Uusitupa, T. Performance of convolutional PML absorbing boundary conditions in finite-difference time-domain SAR calculations. *Phys. Med. Biol.* **2007**, *52*, 7183–7192. [[CrossRef](#)]
44. Smith, B.J.; Kundys, D.; Thomas-Peter, N.; Smith, P.G.R.; Walmsley, I.A. Phase-controlled integrated photonic quantum circuits. *Opt. Express* **2009**, *17*, 13516–13525. [[CrossRef](#)] [[PubMed](#)]
45. Wang, Y.; Tian, Z.; Li, Y.; Zhang, Z.; Wang, L.; Chen, Q. Phase customization in photonic integrated circuits with trimmed waveguides. *Opt. Lett.* **2022**, *47*, 5889–5892. [[CrossRef](#)] [[PubMed](#)]
46. Cooper, M.L.; Mookherjee, S. Numerically-assisted coupled-mode theory for silicon waveguide couplers and arrayed waveguides. *Opt. Express* **2009**, *17*, 1583–1599. [[CrossRef](#)] [[PubMed](#)]
47. Hazura, H.; Menon, P.S.; Majlis, B.Y.; Hanim, A.R.; Mardiana, B.; Hasanah, L.; Mulyanti, B.; Mahmudin, D.; Wiranto, G. Modeling of SOI-based MRR by coupled mode theory using lateral coupling configuration. In Proceedings of the 10th IEEE International Conference on Semiconductor Electronics (ICSE), Kuala Lumpur, Malaysia, 19–21 September 2012; pp. 422–425.
48. Syahriar, A.; Adam, H.; Astharini, D.; Lubis, A.L.; Gandana, D.M. Analysis of three parallel waveguides using coupled mode theory and the method of lines. In Proceedings of the 2016 International Seminar on Application for Technology of Information and Communication, Baku, Azerbaijan, 12–14 October 2016; pp. 174–178.

49. Zhu, S.; Fang, Q.; Yu, M.B.; Lo, G.Q.; Kwong, D.L. Propagation losses in undoped and n-doped polycrystalline silicon wire waveguides. *Opt. Express* **2009**, *17*, 20891–20899. [[CrossRef](#)] [[PubMed](#)]
50. Donzella, V.; Sherwali, A.; Flueckiger, J.; Grist, S.M.; Fard, S.T.; Chrostowski, L. Design and fabrication of SOI micro-ring resonators based on sub-wavelength grating waveguides. *Opt. Express* **2015**, *23*, 4791–4803. [[CrossRef](#)] [[PubMed](#)]
51. Fu, Y.; Hu, X.; Lu, C.; Yue, S.; Yang, H.; Gong, Q. All-optical logic gates based on nanoscale plasmonic slot waveguides. *Nano Lett.* **2012**, *12*, 5784–5790. [[CrossRef](#)]
52. Li, M.; Li, C.; Chen, Y.; Feng, L.; Yan, L.; Zhang, Q.; Bao, J.; Liu, B.; Ren, X.; Wang, J.; et al. On-chip path encoded photonic quantum Toffoli gate. *Photon. Res.* **2022**, *10*, 1533–1542. [[CrossRef](#)]
53. Klauck, F.; Heinrich, M.; Szameit, A. Photonic two-particle quantum walks in Su–Schrieffer–Heeger lattices. *Photon. Res.* **2021**, *9*, A1–A7. [[CrossRef](#)]
54. Zhang, Q.; Li, M.; Xu, J.; Lin, Z.; Yu, H.; Wang, M.; Fang, Z.; Cheng, Y.; Gong, Q.; Li, Y. Reconfigurable directional coupler in lithium niobate crystal fabricated by three-dimensional femtosecond laser focal field engineering. *Photon. Res.* **2019**, *7*, 503–507. [[CrossRef](#)]
55. Anton, C.; Loredò, J.C.; Coppola, G.; Ollivier, H.; Viggianiello, N.; Harouri, A.; Somaschi, N.; Crespi, A.; Sagnes, I.; Lemaitre, A.; et al. Interfacing scalable photonic platforms: Solid-state based multi-photon interference in a reconfigurable glass chip. *Optica* **2019**, *6*, 1471–1477. [[CrossRef](#)]
56. Atzeni, S.; Rab, A.S.; Corrielli, G.; Polino, E.; Valeri, M.; Mataloni, P.; Spagnolo, N.; Crespi, A.; Sciarrino, F.; Osellame, R. Integrated sources of entangled photons at the telecom wavelength in femtosecond-laser-written circuits. *Optica* **2018**, *5*, 311–314. [[CrossRef](#)]
57. Wei, D.; Wang, C.; Wang, H.; Hu, X.; Wei, D.; Fang, X.; Zhang, Y.; Wu, D.; Hu, Y.; Li, J.; et al. Experimental demonstration of a three-dimensional lithium niobate nonlinear photonic crystal. *Nat. Photon.* **2018**, *12*, 596–600. [[CrossRef](#)]
58. Marshall, G.D.; Politi, A.; Matthews, J.C.F.; Dekker, P.; Ams, M.; Withford, M.J.; O’Brien, J.L. Laser written waveguide photonic quantum circuits. *Opt. Express* **2009**, *17*, 12546–12554. [[CrossRef](#)] [[PubMed](#)]

Disclaimer/Publisher’s Note: The statements, opinions and data contained in all publications are solely those of the individual author(s) and contributor(s) and not of MDPI and/or the editor(s). MDPI and/or the editor(s) disclaim responsibility for any injury to people or property resulting from any ideas, methods, instructions or products referred to in the content.